Available online at www.sciencedirect.com
ScienceDirect
Journal of the European Ceramic Society 29 (2009) 2177–2184
www.elsevier.com/locate/jeurceramsoc

# Mechanical properties of textured ceramics from muscovite–kaolinite alternate layers

F. Gridi-Bennadji [a], D. Chateigner [b], G. Di Vita [a], P. Blanchart [a,*]

[a] *GEMH, ENSCI, Av. A. Thomas 87065 Limoges, France*
[b] *CRISMAT-ENSICAEN, UMR CNRS n° 6508, Université de Caen Basse-Normandie, bd. M. Juin, 14050 Caen, France*

Received 10 September 2008; received in revised form 16 December 2008; accepted 8 January 2009
Available online 4 February 2009

**Abstract**

An organized network of mullite anisotropic crystals embedded in a silico-aluminate matrix material is obtained at interfaces of sintered alternate layers of muscovite and kaolinite minerals. The nucleation and growth of mullite anisotropic crystals occur preferentially along the muscovite basal planes through topotactic reaction with the high temperature form of muscovite.

Simultaneously to structural transformations, dehydroxylation of muscovite induces an exfoliation process, which is temperature and time dependent. The kinetics of this process was controlled using an appropriate thermal cycle and uniaxial load. During sintering, the control of mullite size mainly depends in temperature and the addition of a small quantity of low-temperature liquid phase also favors the growth of mullite. But liquid induces the weakening of the organization degree of the mullite network. Quantitative texture analysis (QTA) and SEM were used to characterize microstructural characteristics.

Flexural strength, Young modulus and fracture toughness are closely related to size and organization degree of the mullite network. In general, mullite length favors the increase of strength and fracture toughness. But a high organization degree of the mullite network favors the occurrence of interconnected crystals and increases mechanical properties.


*Keywords:* Mullite; Muscovite–kaolinite alternate layers; Textured ceramics

## 1. Introduction

Ceramics with an organized microstructure are extensively studied because of their potentialities in obtaining very specific behaviors. Particularly, the mechanical behavior can be very different from that of monolithic ceramics, which exhibit a brittle fracture behavior and low fracture toughness. To improve applications under contact damage conditions, many attempts for the fabrication of multilayer ceramic composites with a tailored microstructure have been proposed. An example of a recent study[1] demonstrates that alumina/alumina laminar composites with alternatively oriented crystallites in layers present a high bending strength, which depends on the direction of the multilayered microstructure. In a different way, oxide–oxide laminated composites with aluminum phosphate and alumina platelets were developed by the tape casting method.[2] The bending strength and the work of fracture are improved since cracks are deflected along the alumina interphase layers. Also, the preparation and mechanical properties of machinable alumina/mica composites were studied.[3] The microstructure exhibits large and anisotropic mica crystals, which influence the strength and the fracture toughness of the composite.

Similar materials like layered ceramics are designed of thin layers with specific interfaces. Under load, cracks propagate firstly along the interfaces. If the importance of crack deflection is sufficient to cause splitting between layers, a damage-tolerant response and a nonlinear fracture behavior are obtained.[4]

In organized ceramics with oriented microstructures, the degree of orientation can be achieved using many processes including adding seed particles,[5,6] epitaxial crystal growth on various substrates[7,8] or by the in situ formation of anisotropic grains by the template technique.[9,10] In this study, we use large muscovite flakes, a phyllosilicate mineral from the mica group.[11] During the thermal cycle for sintering, the structural characteristics of muscovite are maintained, but mainly at low distance.[7]

* Corresponding author.
*E-mail address:* philippe.blanchart@unilim.fr (P. Blanchart).

0955-2219/$ – see front matter © 2009 Elsevier Ltd. All rights reserved.
doi:10.1016/j.jeurceramsoc.2009.01.004

This residual structural order of high temperature muscovite favors the epitaxial growth of mullite crystals.

During recrystallization, a small quantity of liquid highly favors the mullite formation at a moderate temperature, typically below 1200 °C. Crystal growth is favored by local concentrations of a transient liquid phase at interfaces, which enhance the mobility of species. Many elements favor the liquid formation, but the addition of $Bi^{3+}$ appears to be a promising way for mullite formation in ceramic compositions[12] and for the reduction of the formation temperature.[13]

The aim of this study is to correlate the characteristics of microstructures of multilayered ceramics to their mechanical properties. Layered ceramics are obtained by the stacking of kaolinite–muscovite alternate layers and a subsequent sintering operation. Both the size and the degree of organization of mullite acicular crystals are considered in the microstructures. The mechanical properties, i.e. the bending strength and the fracture toughness, are necessary properties to be considered during the service of layered ceramics.

## 2. Experimental

In this study, we used large muscovite flakes (20–50 mm) from Bihar (India).[14] The structural characteristics and chemical composition are very close to tabulated data for $2M_1$ muscovite.[15]

The kaolinite is the very high purity and reference material kga-1b from the Clay Mineral Society (University of Missouri, USA).[16] This raw material is well known and exhibits very reproducible chemical and mineralogical compositions.

Layered composites were elaborated with large muscovite flakes (20–50 mm) covered by a thin deposit of kaolinite. Kaolinite–muscovite mass ratio was maintained close to 1. Kaolinite was deposited using a concentrated aqueous suspension (40 vol%) obtained by ball grinding the kaolinite powder in water. While this former series of samples was prepared without any addition, a second series of experiments was operated with Bismuth nitrate addition (5 mol%) in the aqueous slurry.

After kaolinite deposition, the obtained layers were stacked under uniaxial load and the resulting samples dried at 100 °C during 2 h.

A specific sintering process must be optimized to obtain dense samples because porosity develops during muscovite dehydroxylation, due to the in situ combination process of hydroxyls, which forms water vapor and favors the layer expansion.[17] The formation of porosity is counterbalanced by the control of the sintering kinetics under uniaxial load.

The sintering densification was studied in a recording dilatometer. In the 800–1100 °C range, the high densification rate of dehydroxylated minerals is limited by mullite crystallization and growth, while above 1100 °C, a significant densification is observed under the influence of the peritectic reaction at 1140 °C, in the $SiO_2$–$Al_2O_3$–$K_2O$ ternary diagram. The presence of liquids favors creep variations and from creep–temperature relationships, an optimized thermal cycle was obtained (Fig. 1).

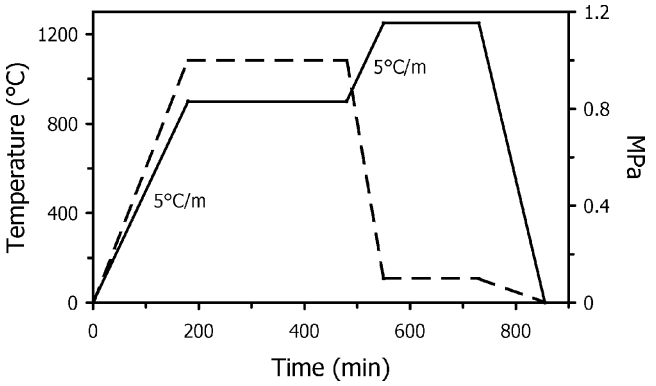


Fig. 1. Optimized thermal cycle for the sintering of muscovite–kaolinite composites.

Microstructural observations were performed on polished surfaces of the in-plane (perpendicular to the pressure direction) and cross-sections (parallel) of the layer stack. Polished samples were chemically etched at room temperature and coated with gold for SEM observations in the backscattering mode. Mullite grain sizes were obtained by image analysis on several SEM images to ensure their statistical significance.

Quantitative texture analysis (QTA) was performed using a four-circle diffractometer equipped with a curved position-sensitive detector (INEL CPS 120) allowing rapid acquisition of the whole diffraction pattern up to 110° 2θ, for each tilt angle $\chi$ and azimuth angle $\varphi$ of the flat sample orientation. The copper monochromatic Kα wavelength was used. Each of the 834 diffraction diagrams acquired for as many sample orientations (using a $5° \times 5°$ measuring grid in $(\chi,\varphi)$ up to $\chi = 55°$) was measured for 120 s. The whole dataset was then analysed using the Rietveld analysis within the combined analysis formalism,[18] in which the orientation distribution function was refined using the E-WIMV approach.[19] Pole figures are plotted using an equal area projection on the sample plane, and are normalized into distribution densities in multiple of a random distribution (m.r.d.). Using such units, a sample without texture exhibits homogeneous pole figures with 1 m.r.d. level, while a textured sample shows minima and maxima in the pole figures ranging from 0 m.r.d. (absence of crystals oriented in this direction) to infinity (for a single crystal on few directions). The overall texture strength is evaluated through the texture index.[18] Such normalisation of the pole figures into m.r.d. values is operated during the orientation distribution (OD) refinement of crystallites during the E-WIMV step. The OD and profile refinement reliabilities are estimated using conventional reliability factors.[20]

The mechanical characteristics were obtained with the flexural strength (Lloyd instrument) at 0.5 mm/min and displacement data were corrected from machine stiffness using strain gauges. The fracture toughness $K_{IC}$ was obtained from Vickers indentation perpendicular to stacked layers and on polished surface. Several measurements were performed after various polishing times, to ensure the validity of measurements. The calculation of fracture toughness uses a well-known approach,[21] since

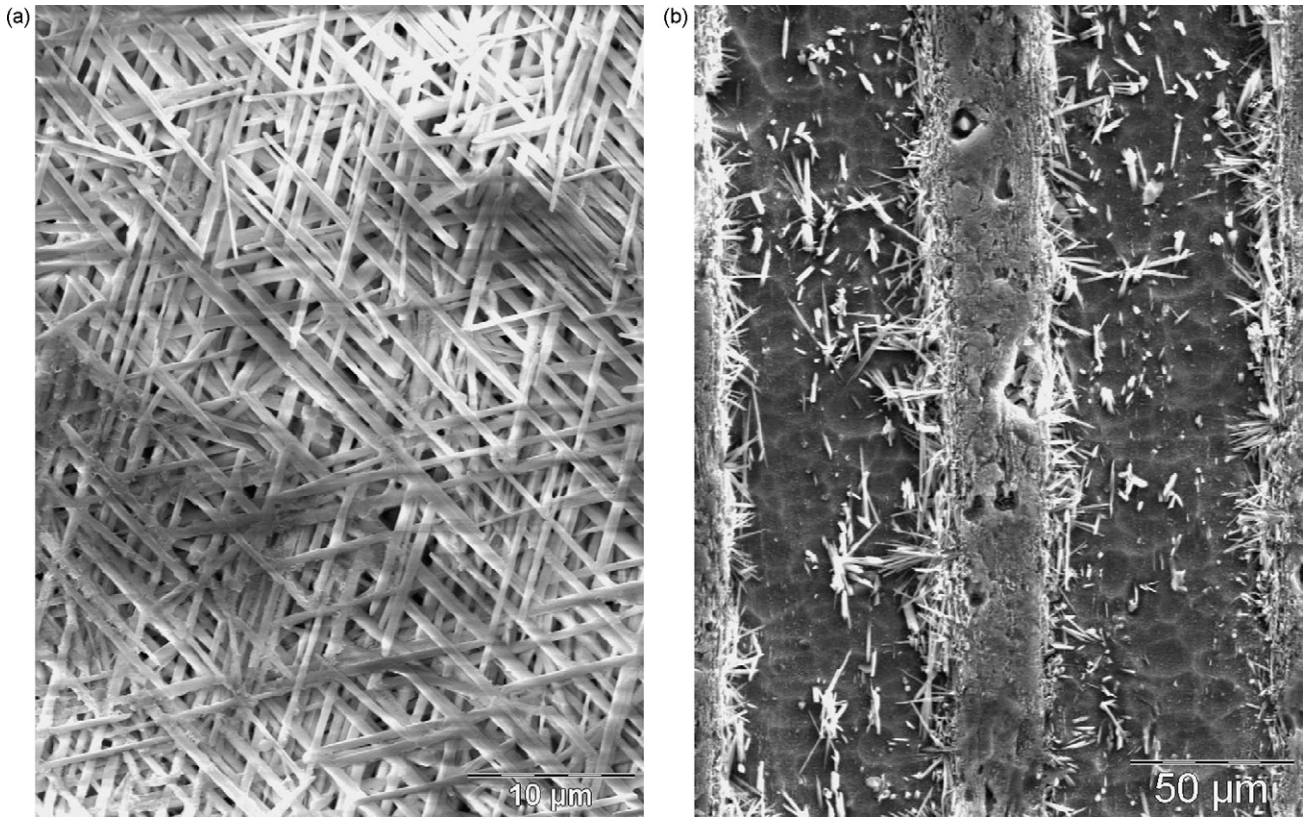


Fig. 2. SEM images of a kaolinite–muscovite composite sintered at 1250 °C. (a) In-plane observation with mullite; (b) cross-section where mullite layers oriented in-plane (bright zone) are separated by two dark silico-aluminate layers.

Palmqvist cracking is observed[22]:

$$K_{IC} = 0.016\left(\frac{E}{H_V}\right)^{0.5} Pc^{-1.5} \quad (1)$$

where $E$ is the elastic modulus, $H_V$ the Vickers hardness, $P$ the measurement load and $c$ is the cracking length. Measurement parameters were optimized[23,24] (load of 15 N during 30 s) to obtain reproducible measurements.

## 3. Results

In the optimized sintering conditions of Fig. 1, SEM photo of Fig. 2a shows dense and well-crystallized materials with mullite crossed-needles oriented in-plane of initial muscovite layers. The cross-section of Fig. 2b shows the layered microstructures with alternate mullite layers and low-organized silico-aluminate layers. The specific recrystallization process of mullite leads to well-organized microstructures with mullite acicular crystals, which form roughly triangular and interpenetrated nets, perpendicularly to the pressure axis as expected from this anisotropic shape.

During sintering, chemical interactions occur above 1140 °C, in accordance to the equilibrium phases in the $SiO_2$–$Al_2O_3$–$K_2O$ system. Possible equilibrium phases are cristobalite, leucite, orthoclase and mostly mullite. The X-ray diffraction pattern (Fig. 3) of a sample sintered at 1200 °C evidences the presence of mullite and γ-alumina, in accordance to possible reaction paths observed during the high temperature transformation of kaolinite[25] and muscovite.[26] Besides, an amorphous phase is evidenced, which originates from the high temperature liquid. In general, the liquid favors the recrystallization of new phases as mullite and cristobalite, but this transformation occurs very progressively at 1200 °C. With our material, the increase in liquid quantity also changes the recrystallization process, which results in a poorly ordered microstructure.

We choose to enhance the mullite recrystallization process at low temperature (∼1000 °C) with the addition of a small quantity of $Bi_2O_3$, since its role on liquid formation at about 1000 °C was demonstrated in silico-aluminates materials.[12,13] With $Bi_2O_3$ addition, the sample microstructure for a 1250 °C

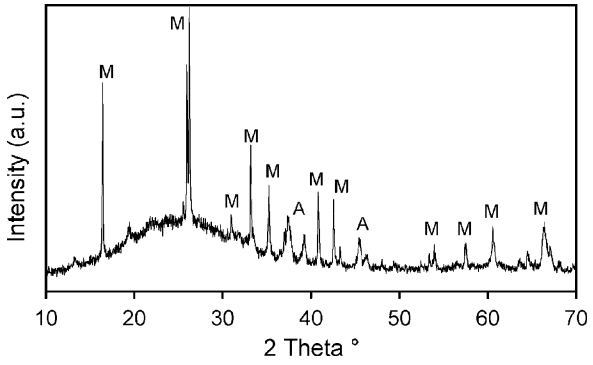


Fig. 3. Typical X-ray diffraction pattern of a kaolinite–muscovite composite sintered at 1200 °C. M: mullite, A: γ-alumina.

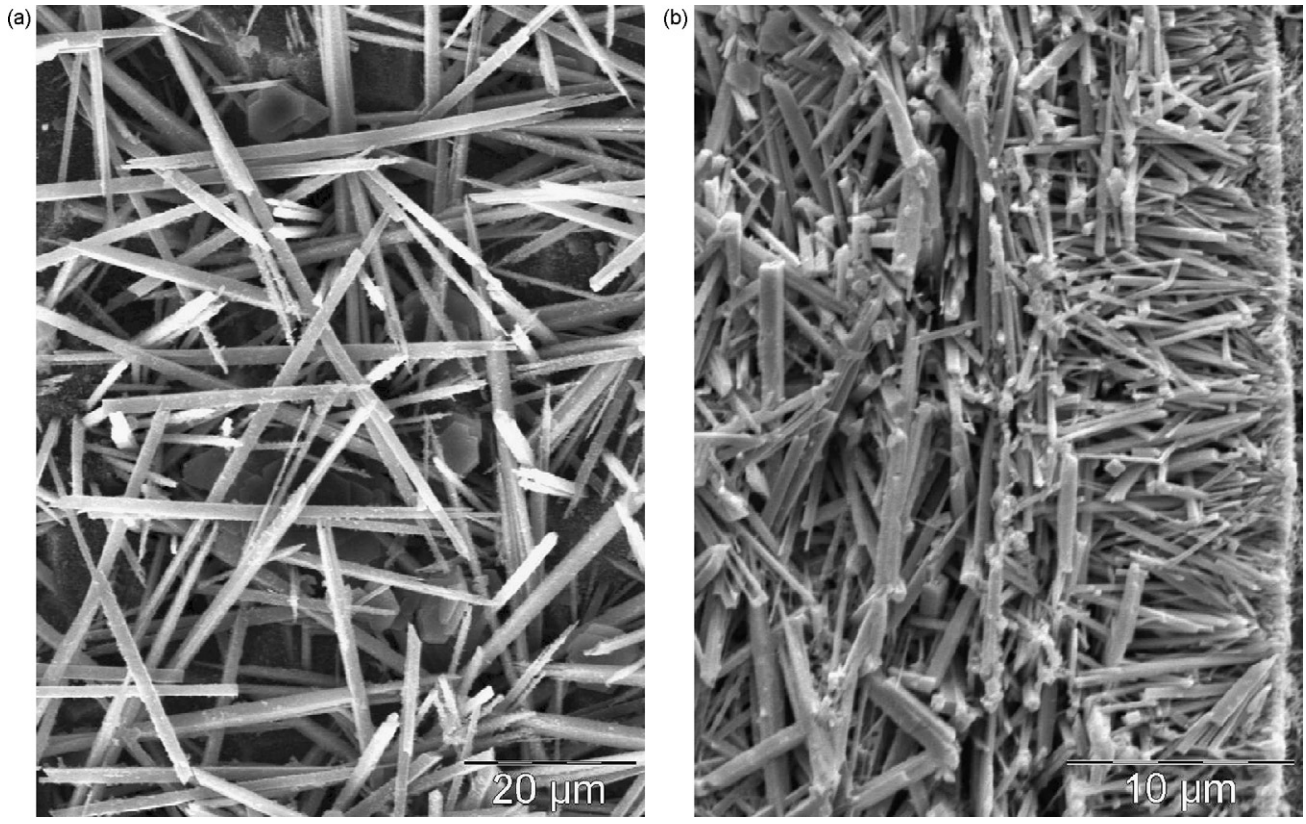


Fig. 4. In-plane (a) and (b) cross-section backscattering SEM images of a kaolinite–muscovite composite sintered at 1250 °C with 5 mol% of $Bi_2O_3$.

sintering (Fig. 4) exhibits very large grain sizes for mullite, in comparison to the ones obtained without addition (Fig. 2). But simultaneously, a weaker organization of the microstructure is obtained with this modified liquid phase quantity and characteristics.

The results of combined analysis for the sample elaborated without addition reveal that the only phases present in the sample are mullite and an amorphous phase that could be fitted using amorphous silica (Fig. 5a). The fit quality is obtained with good reliability factors of $R_w = 4.87\%$ and $R_B = 4.01\%$ for the OD refinement, and $R_w = 12.90\%$ and $R_B = 10.28\%$ for the Rietveld fit, giving an overall goodness of fit of 1.77. The refined cell parameters are similar to that of mullite ($a = 7.56486(5)$ Å; $b = 7.71048(5)$ Å; $c = 2.89059(1)$ Å) as determined by other authors.[27,28] The {0 2 0}, {2 0 0} and {0 0 1} pole figures for the main indices of this sample (Fig. 5b) show as a main texture component, that is a planar texture with ⟨0 0 1⟩ directions aligned roughly at random in the sample plane, i.e. perpendicular to the pressure axis. All other crystallographic directions are at random around the *c*-axes. Another minor preferred orientation component is seen in the centre of the {2 0 0} pole figure, indicating a fiber texture with *a*-axes of mullite defining the fiber axis perpendicular to the sample plane. The two texture components achieve a maximum of 1.8 m.r.d. on the {2 0 0} pole figure and around 1.39 m.r.d. at the periphery of the {0 0 1} pole figure, with an OD texture index of 1.2 m.r.d,[2] revealing the overall weakly stabilised texture strength. Looking closer at the {0 0 1} pole figure, one can identify a series of six {0 0 1} poles located at $\chi = 60°$ each other around the sample normal, as a sign of a subsidiary organization of the *c*-axes in the sample plane (Fig. 5c). On this figure the 0.68 minimum density indicates that 68% of the crystals are not oriented with their *c*-axes corresponding to the mean orientation component. These pole reinforcements are to be correlated with the triangular network seen on SEM images, and are coherent with long mullite crystal axes corresponding to ⟨0 0 1⟩.

The size of mullite crystals (Fig. 6) as deduced from image analysis of the SEM pictures indicates that the average length of mullite anisotropic crystals (*c*-axes) increases with temperature, for both material series. When $Bi_2O_3$ is added, a significant increase of mullite crystal lengths (Fig. 6) is obtained for all temperatures and a bit more pronounced for the lowest ones, around 1200 °C. Simultaneously, size distribution broadens with temperature (Fig. 6). From microstructure observations, it is shown that mullite size and organization degree can be controlled with either the thermal cycle and the liquid phase quantity or composition with Bismuth. It is illustrated in SEM photos where either a well-organized microstructure (Fig. 2) or a weakly organized microstructure (Fig. 4) are obtained using the same thermal cycle.

The stress–strain characteristics during flexural measurements evidence an elastic behavior up to fracture (Fig. 7). The Young elastic modulus *E* is obtained with the slope of the straight-line portion of the stress–strain characteristics below the maximum stress.

A typical indentation measurement perpendicular to stacked layers is in Fig. 8. Since spot size and cracking length are larger than layer thickness (Figs. 2b and 4b), it shows that the inden-

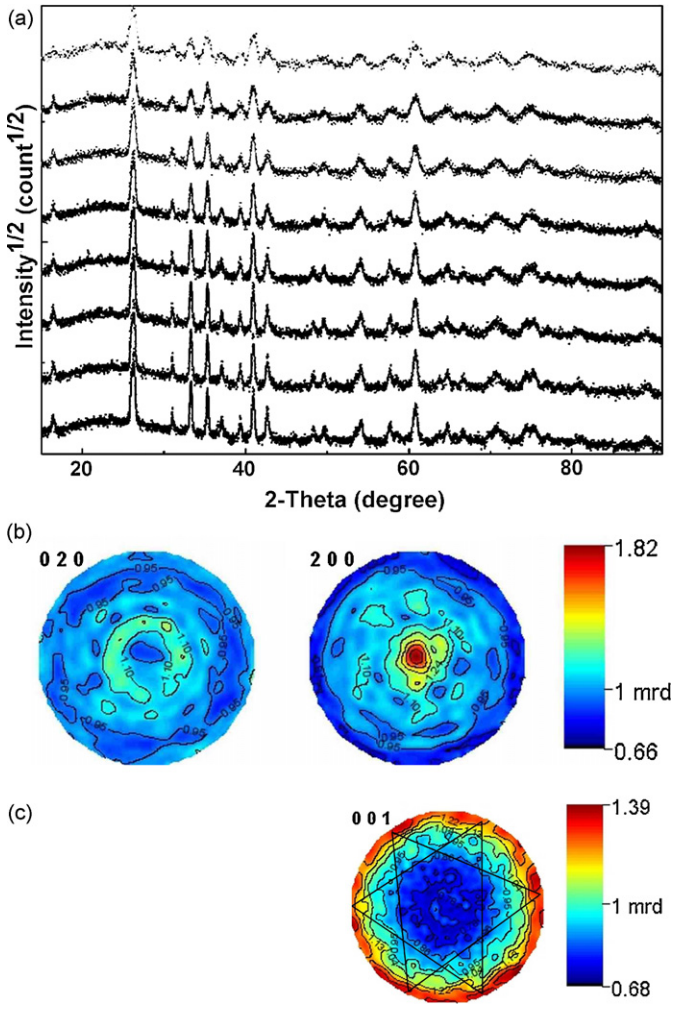


Fig. 5. (a) Selected X-ray diffraction diagrams over the 834 measured to illustrate the fit quality. (b) Recalculated-normalized {0 2 0}, {2 0 0} and {0 0 1} pole figures for the main axes of mullite. (c) {0 0 1} Pole figure represented on its own min–max scale density bar to show the pole reinforcements linked to the in-plane triangular-like organization of the mullite needles. Pole figures are plotted on a linear density scale.

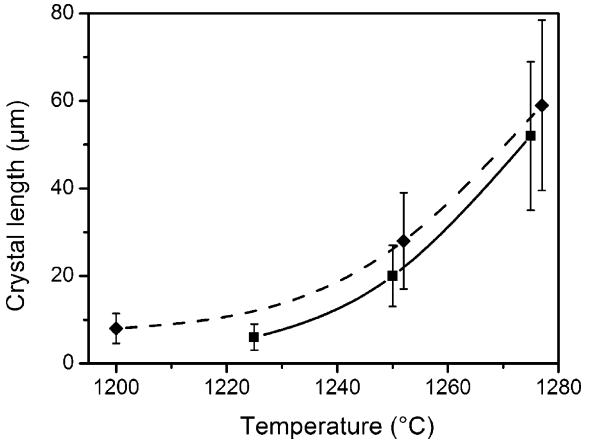


Fig. 6. Mullite crystal length for well (continuous line) and weakly (dashed line) organized materials.

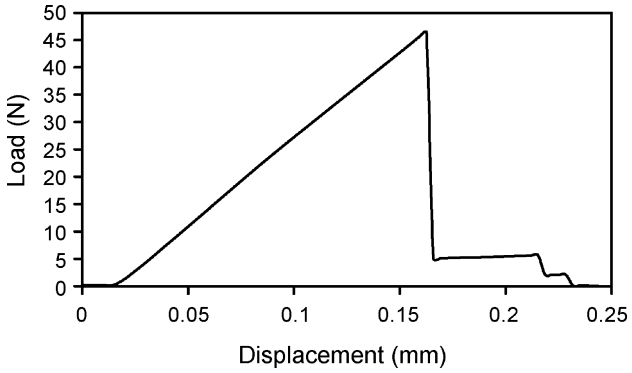


Fig. 7. Typical stress–strain characteristic during flexural measurements. The flexural strength is obtained at the maximum value.

tation measurements relate to the microscopic behavior. The fracture toughness is calculated with the basic equation (1) where the Young modulus and hardness are important parameters. But it was shown that the hardness is load-dependent[29] as in the case of most of ceramic materials. We used a high indentation load (15 N), which can be considered to give load-independent hardness values. The crack length-$K_{IC}$ variation was observed as a function of load and we used plateau values.

Such characterization of materials points out the influence of mullite crystal length in flexural strength (Fig. 9) and fracture toughness (Fig. 10). For a well-organized material, $R_m$ varies from 33 MPa to 58 MPa and $K_{IC}$ from 0.78 MPa m$^{1/2}$ to

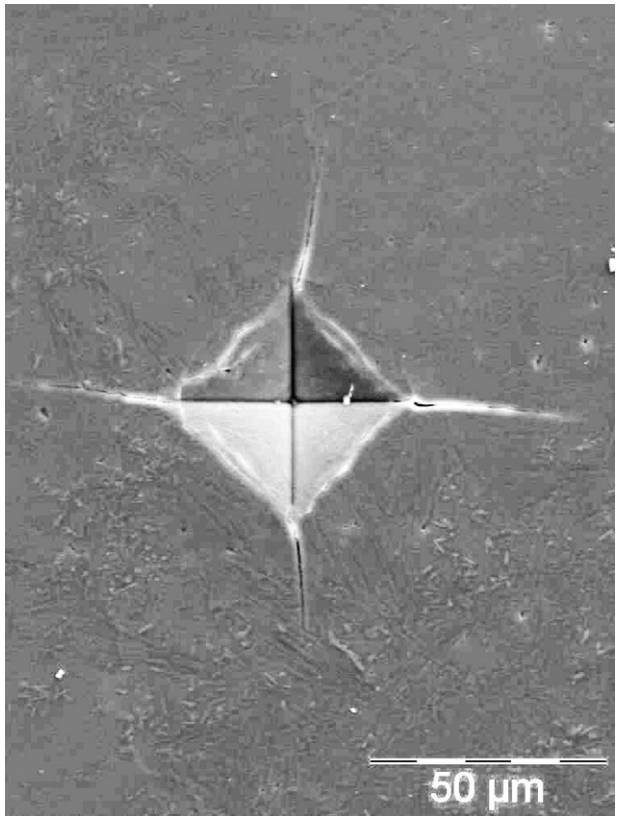


Fig. 8. SEM photo of a typical Vickers indentation measurement perpendicular to stacked layers.

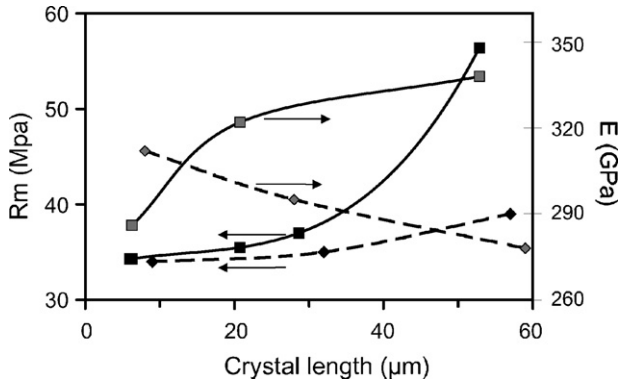


Fig. 9. Bending strength and Young modulus $E$ as a function of mullite crystal length for well (continuous line) and weakly (dashed line) organized materials.

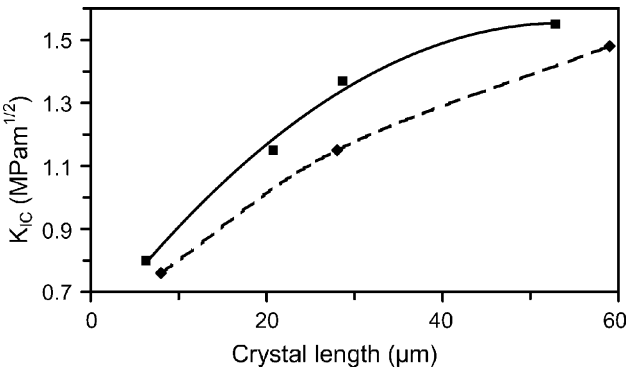


Fig. 10. Fracture toughness as a function of mullite crystal length for well (continuous line) and weakly (dashed line) organized materials.

1.53 MPa $m^{1/2}$ when mullite crystal size increases from 6 μm to 54 μm. In the case of a poorly ordered composite, whereas mullite crystal length vary significantly (8–58 μm), $R_m$ is quasi unchanged (33–38 MPa) but $K_{IC}$ increases in a similar way to the behavior of well-organized materials.

In Fig. 9, the Young modulus of well-organized materials is high (283–332 GPa) and increases with mullite crystal length. For a disorganized material, a decrease of $E$ is observed in spite of a larger mullite size.

## 4. Discussion

Muscovite is one of the most common phases in the micas mineral group. It is a 2:1 layer silicate formed from a sandwich of two tetrahedral layers: sheets of linked [$SiO_4$] tetrahedrons and joined by a layer of $Al^{3+}$ in octahedral coordination.

A typical reaction during thermal transformation of muscovite is the progressive dehydroxylation in a wide temperature interval, 800–1100 °C with a very broad endothermic reaction.[30] This phenomenon is structural dependent and highly crystallized minerals having large crystal sizes retain a part of OH groups up to 1100 °C.[31] The dehydroxylation is accompanied by a progressive crystal structure transformation of muscovite up to 1140 °C, to form an increasingly disorganized structure. A specific feature is the retaining of the global layered organization of muscovite up to this temperature. The Al coordination change from 6 to 5 above 650 °C induces some structural changes but a limited order over a few silica or alumina units is maintained. In the alumina sheet, assemblies of connected alumina cells are oriented towards $[0\,1\,0]_{musc}$ or $[3\,1\,0]_{musc}$ and $[\bar{3}\,1\,0]_{musc}$, which are also the orientations of tetrahedral units of the room temperature muscovite. In spite of a temperature increase up to 1095 °C, the previous preferential directions of Al unit pairs are maintained. The same orientations are also observed with silica cells in the silica sheets.

Elementary chains for the nucleation of new phases are therefore formed. Particularly, mullite nucleates and grows along the above-mentioned preferential directions. Consequently in the mullite structure, which shows chains of edge sharing octahedrons along the $c$-axis, cross-linked by Si and Al tetrahedrons, the $[0\,0\,1]_{mull}$ axis matches the $[0\,1\,0]_{musc}$, $[3\,1\,0]_{musc}$ and $[\bar{3}\,1\,0]_{musc}$ axes of the previously formed muscovite. A detailed description of structural characteristics is in [31].

In kaolinite–muscovite materials without bismuth oxide addition, the microstructure changes strongly with temperature. At the lowest sintering temperature (1225 °C), the mullite crystal size is small, resulting in a weakly interconnected mullite network. It limits the flexural strength and Young modulus. The same tendency is observed for the macroscopic $K_{IC}$ since the size of Vickers indentation imprints (~40 μm) is larger than the mullite crystal size. When the sintering temperature increases at 1250–1275 °C, the microstructures become well organized and mullite crystal lengths are large enough to create an interconnected network (Fig. 2a). It results in increased mechanical characteristics (Figs. 9–10).

When bismuth oxide is added to favor the liquid phase role during sintering, the organization degree of the microstructure decreases simultaneously to the increase of mullite crystal size (Fig. 4). The mechanical strength does not change significantly with the mullite size, but the fracture toughness attains 1.5 MPa $m^{1/2}$ for a mullite crystal length of 58 μm. It means that the flexural strength is strongly related to the existence of interconnection in the mullite network. But the fracture toughness rather depends on the diagonal length of the indentation impression and the length of the indentation cracks. Since these dimensions are similar to that of the mullite crystal size, the indentation results are considered to represent the local behavior.

The Young modulus is changed with mullite crystal length and organization. In the case of organized materials, $E$ increases with mullite crystal size (from 283 GPa to 332 GPa) while it decreases for weakly organized materials (from 313 GPa to 278 GPa), simultaneously to the reduction of the texture degree of crystallites. As for the flexural strength, the existence of an interconnected network of mullite crystals is a necessary condition to increase the Young modulus.

We suggest that the mechanical behavior of our layered composite materials is mainly controlled by the distribution of dislocation sources through alternate regions with different elastic–plastic behaviors.[32] Fig. 2b shows the alternate layers with different microstructures: (a) mullite layers oriented in-plane (bright zones in Fig. 2a) and (b) which alternates with amorphous layers (dark zones in Fig. 2b). The significant difference in layer microstructures leads to different mechan-

ical behaviors. Particularly, a more accentuated elastic–plastic behavior of the amorphous layers can be assumed. During crack propagation, the amount of the energy dissipation in the amorphous layers influences the fracture toughness and the flexural strength. But mechanical properties are also influenced by the size and the number of layers because possible residual thermal stresses[33] influence crack propagation.

In the case of a weakly organized material, as presented with the cross-section of Fig. 4, the mechanisms mentioned above do not occur. The global behavior of the layered material is similar to that of a bulk (not layered) ceramic material. It means that an optimal architecture must be performed to maximize material toughness and strength,[34] but further technological challenges still remain to control both physical properties of layers and interfaces as exact thickness of layers over a large distance.

Finally, our results can be compared to porcelain data, a microcomposite material with mullite needles in a glassy matrix.[35] The average size of mullite in porcelain is about 5 μm, with typical strength of 42 MPa and fracture toughness of 0.7 MPa $m^{1/2}$. This means that our materials exhibit interesting mechanical properties than that of similar silico-aluminate materials, which need sintering at higher temperature. Comparing this way, we point on a potential replacement of porcelain pieces by a new composite. Potential applications are stronger and less brittle silicates ceramics for a large range of applications.

## 5. Conclusion

The layered material has a microcomposite microstructure with mullite layers, which alternate with low organized material layers. The sintering process is a key point to control both the material density and high material density is obtained since the sintering kinetic is controlled by a suitable thermal cycle and a uniaxial pressure during sintering. In microstructure, the size and organization degree of mullite crystallites are mainly controlled by both sintering temperature and time. But the addition of a small quantity of liquid phase at low temperature, with bismuth oxide, favors the increase of mullite size and the weakening of the organization degree of the mullite network. We evidence that it is possible to control the microstructural characteristics in the composite materials.

Mechanical properties are characterized with the flexural strength, the Young modulus and the fracture toughness from Vickers indentation. A close relationship is observed between mechanical characteristics and size and organization degree of the mullite crystals. In particular, the mullite length along the *c*-axis is determinant to strength and fracture toughness, but simultaneously, the organization degree of mullite must be as high as possible. This tendency was confirmed with well-organized materials, which microstructure was characterized by X-ray diffraction and QTA, and by electronic microscopy. In the case of poorly ordered microstructures, whereas mullite length attains high values, the flexural strength is limited to values similar to that of bulk materials. It is proposed that not only high mullite length is necessary to increase strength, but also the existence of an interconnected network of crystallite.

## Acknowledgements

The authors would like to express their gratitude towards the European Community (the European Social Funds) and the Limousin Region for their financial support of the present work.

## References

1. Suzuki, T. S., Uchikoshi, H., Okuyama, Y., Sakka, K. and Hiraga, K., Mechanical properties of textured, multilayered alumina produced using electrophoretic deposition in a strong magnetic field. *Journal of the European Ceramic Society*, 2006, **26**, 661–665.
2. Kim, D. K. and Kriven, W. M., Oxide laminated composites with aluminum phosphate ($AlPO_4$) and alumina platelets as crack deflecting materials. *Composites: Part B*, 2006, **20**, 1–6.
3. Taruta, S., Fujisawa, R. and Kitajima, K., Preparation and mechanical properties of machinable alumina/mica composites. *Journal of the European Ceramic Society*, 2006, **26**, 1687–1693.
4. Watts, J. and Hilmas, G., Crack deflection in tungsten carbide based laminates. *International Journal of Refractory Metals & Hard Materials*, 2006, **24**, 222–228.
5. Hong, S.-H. and Messing, G. L., Development of textured mullite by templated grain growth. *Journal of the American Ceramic Society*, 1999, **82**(4), 867–872.
6. Chaud, X., Meslin, S., Noudem, J., Harnois, C., Porcar, L., Chateigner, D. *et al.*, Isothermal growth of large YBaCuO single domains through an artificial array of holes. *Journal of Crystal Growth*, 2005, **275**, e855–e860.
7. Lecomte, G. and Blanchart, P., Textured mullite at muscovite–kaolinite interface. *Journal of Materials Science*, 2006, **41**, 4937–4943.
8. Pernet, M., Chateigner, D., Germi, P., Dubourdieu, C., Thomas, O., Sénateur, J. P. *et al.*, Texture influence on critical current density of YBCO films deposited on (1 0 0)-MgO substrates. *Physica C*, 1994, **235**, 627–628.
9. Wang, Z. J., Bi, H. Y., Kokawa, H., Zhang, L., Tsaur, J., Ichiki, M. *et al.*, Preparation and characterization of PZT thin films deposited by pulsed laser deposition on template layer. *Journal of the European Ceramic Society*, 2004, **24**(6), 1629–1632.
10. Guilmeau, E., Itahara, H., Tani, T., Chateigner, D. and Grebille, D., Quantitative texture analysis of grain-aligned $[Ca_2CoO_3]_{0.62}[CoO_2]$ ceramics processed by the reactive-templated grain growth method. *Journal of Applied Physics*, 2005, **97**, 064902.1–064902.7.
11. Bergaya, F., Theng, B. K. G. and Lagaly, G., *Handbook of Clay Science*. Elsevier, 2006.
12. Kong, L. B. and Zhang, T. S., Some main group oxides mullite phase formation and microstructure evolution. *Journal of Alloys and Compounds*, 2003, **359**(1–2), 292–299.
13. Okada, K., Activation energy of mullitization from various starting materials. *Journal of the European Ceramic Society*, 2008, **28**(2), 377–382.
14. Klein, H. H., Stern, W. B., Weber, W. and Switz, B., On physical and chemical properties of ruby muscovite used in the electrical industry. *Schweizerische Mineralogische und Petrographische Mitteilungen*, 1982, **62**(1), 145–173.
15. Liang, J. and Hawthorne, F. C., Rietveld refinement of micaceous materials: muscovite-2M1, a comparison with single-crystal structure refinement. *Canadian Mineralogist*, 1996, **34**, 115–122.
16. Pruett, R. J. and Webb, H. L., Sampling and analysis of KGa-1B well-crystallized kaolin source clay. *Clays and Clay Minerals*, 1993, **41**, 514–519.
17. Gridi-Bennadji, F. and Blanchart, P., Dehydroxylation kinetic and exfoliation of muscovite flakes. *Journal of Thermal Analysis and Calorimetry*, 2007, **90**(3), 747–753.
18. Chateigner, D., ed., *Combined Analysis: Structure–Texture–Microstructure–Phase–Stresses–Reflectivity Analysis by X-ray and Neutron Scattering*, 2004, 152 p. http://www.ecole.ensicaen.fr/~chateign/texture/combined.pdf.

19. Lutterotti, L., Chateigner, D., Ferrari, S. and Ricote, J., Texture, residual stress and structural analysis of thin films using a combined X-ray analysis. *Thin Solid Films*, 2004, **450**, 34–41.
20. Chateigner, D., Reliability criteria in quantitative texture analysis with experimental and simulated orientation distributions. *Journal of Applied Crystallography*, 2005, **38**, 603–611.
21. Niihara, K., Morena, R. and Hasselman, D. P. H., Evaluation of $K_{IC}$ of brittles solids by the indentation method with low crack-to-indent ratios. *Journal of Materials Science Letters*, 1982, **1**, 13–16.
22. Niihara, K., Morena, R. and Hasselman, D. P. H., Indentation fracture toughness of brittle materials for palmqvist cracks. In *Fracture mechanics of ceramics*, *vol. 5*, ed. R. C. Bradt, A. G. Evans, P. P. Hasselman and F. F. Lange. Plenum Press, New York, 1983, pp. 97–105.
23. Ribeiro, A., Pintaude, G. and Sinatora, A., The use of a Vickers indenter in depth sensing indentation for measuring elastic modulus and Vickers hardness. *Materials Research*, 2004, **7**(3), 483–491.
24. Petit, F., Vandeneede, V. and Cambier, F., Relevance of instrumented microindentation for the assessment of hardness and Young's modulus of brittle materials. *Materials Science and Engineering: A*, 2007, **456**(1–2), 252–260.
[25]. Chen, Y-F., Wang, M-C. and Hon, M-H., Phase transformation and growth of mullite in kaolin ceramics. *Journal of the European Ceramic Society*, 2004, **24**, 2389–2397.
26. Mackenzie, K. J. D., Brown, I. W. M., Cardile, C. M. and Meinhold, R. H., The thermal reaction of muscovite studied by high resolution solid state 29-Si and 27-Al NMR. *Journal of Materials Science*, 1987, **22**, 2645–2654.
27. Fischer, R. X., Schmucker, M., Angerer, P. and Schneider, H., Crystal structures of Na and K aluminate mullites. *American Mineralogist*, 2001, **86**, 1513–1518.
28. Crystallography Open Database n°9005501. www.crystallography.net.
29. Gong, J. H., Si, W. J. and Guan, Z. D., Effect of load-dependance of hardness on indentation toughness for soda-lime glass. *Journal of Non-Crystalline Solids*, 2001, **282**, 325–328.
30. Grim, R. E., Bradley, W. F. and Brown, G., In *X-ray Identification and Crystal Structures of Clay Minerals*, ed. G. W. Brindley. Mineralogical Society, London, 1951, pp. 138–172.
31. Gridi-Bennadji, F., Beneu, B., Laval, J. P. and Blanchart, P., Structural transformations of muscovite at high temperature by X-ray and neutron diffraction. *Applied Clay Science*, 2008, **38**(3–4), 259–267.
32. Chen, C. R., Pascual, J., Fischer, F. D., Kolednik, O. and Danzer, R., Prediction of the fracture toughness of a ceramic multilayer composite—modeling and experiments. *Acta Materialia*, 2007, **55**(2), 409–421.
33. Lube, T., Pascual, J., Chalvet, F. and de Portu, G., Effective fracture toughness in $Al_2O_3$–$Al_2O_3$/$ZrO_2$ laminates. *Journal of the European Ceramic Society*, 2007, **27**(2–3), 1449–1453.
34. Bermejo, R., Pascual, J., Lube, T. and Danzer, R., Optimal strength and toughness of $Al_2O_3$–$ZrO_2$ laminates designed with external or internal compressive layers. *Journal of the European Ceramic Society*, 2008, **28**(8), 1575–1583.
35. Iqbal, Y. and Lee, W. E., Microstructural evolution in triaxial porcelain. *Journal of the American Ceramic Society*, 2000, **83**(12), 3121–3127.